Journal of Polymers and the Environment
https://doi.org/10.1007/s10924-019-01512-0

ORIGINAL PAPER

Effect of the Processing-Induced Morphology on the Mechanical Properties of Biodegradable Extruded Films Based on Poly(lactic acid) (PLA) Blends

Mathilde Siccardi[1,2] · Xoan Xosé Garcia-Fonte[3] · Antoine Simon[1,2] · Valeria Pettarin[4] · María José Abad[3] · Celina Bernal[1,2]

Abstract
Biodegradable films based on poly(lactic acid) blends were obtained by cast extrusion. Their tensile and fracture behavior was investigated and the effect of the processing conditions through the extrusion rolling speed on this behavior was analyzed. In uniaxial tensile tests, all films presented completely ductile behavior exhibiting a defined yield point, strain softening after this point and a plateau before fracture. Fracture behavior was determined through quasi-static fracture tests on deeply double edge notched tensile specimens. The film obtained at the lowest rolling speed exhibited completely ductile behavior hence, the Essential Work of Fracture methodology was applied to characterize its fracture. The film processed at intermediate rolling speed, on the other hand, presented ductile fracture or ductile instability depending on the ligament length and the film obtained with the highest rolling speed exhibited a transition regime fracture. In order to compare the fracture behavior of the different films, the *J*-integral at maximum load J_{max} was adopted. Differences in the films fracture behavior were correlated to the processing-induced morphology.

Keywords Biodegradable polymers · Poly(lactic acid) · Polymer blends · Mechanical properties · Processing-induced morphology

Introduction

Recently, in order to reduce environmental impact of petrochemical-based synthetic polymers, many efforts have been devoted to replace them by their biodegradable counterparts. Poly(lactic acid) (PLA) has emerged as an attractive alternative to synthetic polymers, especially in applications with high level of residual materials such as packaging (bags, films, wrappers, containers, etc.). Initially, the main uses of PLA have been limited to medical applications such as implant devices, tissue scaffolds and others, because of polymer high cost, low availability and limited molecular weight. In the last years, the economical production of high molecular weight PLA has decisively contributed to its larger utilization, and PLA has gained huge attention as an alternative to polymers derived from fossil fuels [1].

PLA is a semicrystalline thermoplastic aliphatic polyester synthetized from L-lactic acid obtained from starch fermentation and hence, derived from completely renewable resources. It has a glass transition temperature T_g near to 60 °C and a melting temperature T_m close to 155 °C.

The degree of crystallinity of PLA is related to the amount of D-lactic enantiomer as well as to the molecular weight [2]. PLA commercial grades typically have very low amounts of D-lactic enantiomer, and so the crystallization rate from the melt is quite low if compared with the cooling

✉ Celina Bernal
cbernal@fi.uba.ar

1 Universidad de Buenos Aires, Facultad de Ingeniería, Buenos Aires, Argentina

2 Grupo de Propiedades Mecánicas y Fractura, Instituto de Tecnología en Polímeros y Nanotecnología (ITPN-UBA-CONICET), Universidad de Buenos Aires, Facultad de Ingeniería, Av. Las Heras, 2214, C1127AAR Buenos Aires, Argentina

3 Grupo de Polímeros, Universidad de A Coruña, Centro de Investigaciones Tecnológicas, Escuela Universitaria Politécnica, Av. 19 de Febrero s/n, 15405 Ferrol, Spain

4 Grupo de Ciencia e Ingeniería de Polímeros, INTEMA (UNMdP-CONICET), Av. Colón 10850, 7600 Mar del Plata, Argentina

Published online: 17 July 2019

rates found in frequent transformation processes. Hence, under commonly used processing conditions, the material is almost amorphous [3, 4] and basically relatively brittle [5].

However, PLA has a broad range of applications due to its ability to be stress crystallized, thermally crystallized, impact modified, filled, copolymerized, and processed in most polymer processing equipment. It can be formed into transparent films, fibers, or injection molded into blow-moldable preforms for bottles. It also presents remarkable organoleptic characteristics and is excellent for food contact and related packaging applications [6]. PLA has been also used in a variety of industrial fields such as automotive, computer, and electric appliances as well as in medical applications [7].

In spite of PLA properties are similar to other petroleum based polymers (as PP, PE or PET), it has some drawbacks as hydrophobicity, slow biodegradation or low toughness for structural uses. PLA blending with other polymers is an easy and cost-effective route to obtain materials that overcome the PLA limitations [8]. In the literature there are many examples of miscible blends as PLA/PMMA [9] and immiscible blends as PLA/polyolefines [10], PLA/styrenic polymers [11], PLA/polyamides [12] or PLA/rubbers [13] which are being investigated for different applications. Another good alternative is to blend PLA with other biodegradable and bioabsorbable polymers. This strategy allows obtaining PLA-based materials with improved properties by also keeping its main advantages.

The fracture behavior and properties of PLA and its blends have been recently investigated by different research groups. Rezgui et al. [14] studied the plastic behavior of PLA by analyzing true stress–strain curves and volume changes upon stretching. They observed that at 50 °C, PLA underwent extensive plastic deformation with a marked yield softening followed by a progressively increasing strain hardening. They also found that volume strain steadily increased over the whole plastic stage. The authors discussed their results on the basis of the microscopic damage mechanisms observed in the stretched state.

Among PLA based blends, those with poly(ε-caprolactone) (PCL) are the most studied ones. Todo et al. [15] developed biodegradable PLA/PCL blends with the aim to improve the fracture behavior of PLA. They reported that the primary toughening mechanisms in PLA/PCL blends were the initiation of dense craze-like damage and subsequent matrix ductile deformation. Later, Todo et al. [16] also investigated the effect of PCL content on the fracture behavior of blends of poly(L-lactide) (PLLA) and PCL from measurements of the critical energy release rate at crack initiation, G_{in}. They found that fracture energy was greatly improved by blending PCL with PLLA. PLLA/PCL blends showed multiple craze formation in the crack-tip region, with elongated fibrils and voids building the crazes. Hence, these damage formations were taken as the primary energy dissipation mechanisms leading to improved fracture energy. On the other side, Takayama et al. [7] studied the effect of annealing on the mechanical properties of PLA/PCL blends. Fracture energy dramatically decreased in these blends due to the suppression of ductile deformation of the spherical PCL phase from annealing. By reducing the size of the spherical PCL phase from the incorporation of lysine triisocyanate (LTI), higher fracture energy was obtained. Also, an annealing process applied to PLA/PCL/LTI strengthened the microstructure, resulting in further fracture energy improvement. More recently, Tuba et al. [17] studied biodegradable blends of poly(D,L-lactide) and poly(ε-caprolactone) with different weight fractions of PCL. Compatibilized blends with L-lysine-diisocyanate and L-lysine-triisocyanate were also investigated to increase the material fracture toughness.

In addition, in order to obtain more durable and longer lifetime materials often required in engineering applications, PLA is not only blended with bio-based or biodegradable polymers but also with commodity and/or engineering plastics. Imre et al. [18] have recently presented a comprehensive investigation of the interactions, structure and properties of blends of PLA with different thermoplastic polymers.

The fracture behavior of PLA and its blends affects their resistance during processing, handling and transport. Hence, it determines the extent to which these biopolymers can replace synthetic polymers in many applications, consequently is of major economic concern [19]. In addition, it is well known that in the case of polymers and also of their blends, one of the main determining factors of the materials' morphology and consequently of the materials' final performance is processing conditions. Although PLA can be processed on standard converting equipment with minimal modifications, its unique properties must be taken into consideration in order to optimize the conversion of PLA to molded parts, films, foams, and fibers, etc. In order to optimize the materials' properties, the knowledge of the relationship between processing-induced morphology and deformation and fracture behavior seems to be essential. Although a significant number of works have been published regarding the fracture behavior of PLA-based blends, as mentioned above, and the effect of processing on thermal and standard mechanical properties [20], the effect of morphology on the mechanical and fracture properties of these blends has not been already completely elucidated.

In the present work, the tensile and fracture behavior of extruded films based on PLA blends was investigated. The effect of the processing rolling speed on this behavior was also analyzed in order to determine the relationship between the processing-induced morphology and the mechanical behavior of the films.

Experimental

Materials

Two significantly different commercial blends of co-polyester and PLA (supplied by NatureWorks) were used: Bio-Flex® 6510 (density = 1.30 g/cm^3; melt flow rate (190 °C/2.16 kg) = 2.5–4.5 g/10 min; Young's modulus (E) = 2600 MPa and tensile strength (σ_u) = 47 MPa from Technical data sheet [21]) and Bio-Flex® F 2110 (density = 1.27 g/cm^3; melt flow rate (190 °C/2.16 kg) = 3–5 g/10 min; E = 730 MPa and σ_u = 20 MPa from Technical data sheet [22]). The Bio-Flex® trade name indicates blends of co-polyesters with a very high content of natural resource material. More specifically, it is a blend of an aliphatic co-polyester (PLA type) and another aromatic one plus processing enhancing additives [23], as observed in FTIR analysis of raw pellets (not shown). The co-polyesters are found in different proportions in Bio-Flex 6510 and Bio-Flex 2110 and this produces the differences in their macroscopic properties A blend with a proportion of 70/30, w/w Bio-Flex 6510/BioFlex F 2110, was prepared in order to obtain different two-phase morphologies in the films.

Processing of PLA Based Films

For the preparation of the extruded films, a Brabender DSE-20 twin-screw extruder with a flat die was used (both barrel and die temperature were 165 °C and the screw speed was 30 rpm). The melted polymer formulation was cooled on a chilled roll and stretched in the machine direction. The chilled roll was kept at 60 °C. In order to induce different morphologies in the films through stretching in the machine direction, several rolling speeds were used: 0.6; 1.8 and 3 rpm. These rolling speeds corresponded to draw ratios of 2.9; 6.3 and 11.1, respectively as determined from area reduction values after film extrusion. Thickness of processed films varied between 0.05 and 0.4 mm.

Microstructure and Morphology Analysis

Thermal measurements were carried out with a differential scanning calorimeter (DSC Pyris 1, from Perkin Elmer) under nitrogen atmosphere. Samples of 6–10 mg were heated from − 20 °C to 200 °C at a heating rate of 10 °C/min, holded 3 min at 200 °C to erase processing-induced structure, cooled to − 20 °C at a heating rate of 10 °C/min, and heated again from − 20 °C to 200 °C at a heating rate of 10 °C/min. The first heating scan was used to determine the processing-induced structure, while the second scan was used to determine the blend's properties without influence of processing.

The glass transition temperature (T_g), cold crystallization temperature (T_c), melting temperature (T_m) and melting enthalpy (ΔH_m) were obtained from the heating scan. Moreover, crystallinity values (x_c) were calculated according to Eq. (1), with ΔH_0 = 93.6 J/g for the melting enthalpy of 100% crystalline PLA [24, 25].

$$x_c = \frac{\left(\Delta H_m - \Delta H_c\right)}{\Delta H_0} \times 100\% \quad (1)$$

Fracture surfaces of cryo-fractured specimens obtained at liquid nitrogen temperature in the longitudinal direction (machine direction) were analyzed by field emission scanning electron microscopy (FE-SEM). Samples were coated with a thin layer of gold before observation.

Mechanical Characterization

Uniaxial Tensile Tests

Uniaxial tensile tests were performed in an Instron dynamometer 5982 on rectangular specimens (ASTM 882-02) cut out from the different films along the longitudinal direction (machine direction) at a crosshead speed of 5 mm/min. Stress–strain curves were obtained and Young's modulus (E), yield strength (σ_y) (maximum stress) and strain at break (ε_b) values were determined from these curves. Young's modulus was calculated according to the slope of the initially linear part of the stress–strain curve. A minimum of four specimens were tested for each system. Average values of the mechanical parameters and their deviations were reported.

Quasi-static Fracture Tests

Quasi-static fracture tests were carried out at 10 mm/min on deeply double edge-notched tension (DDENT) specimens cut along the machine direction (initial notches were introduced in the direction perpendicular to the extrusion direction) in the testing machine. Sample dimensions were: length (Z) = 50 mm and depth (W) = 20 mm. Distance between grips was 30 mm. Two properly aligned sharp notches of varying depth were performed by sliding a fresh razor blade into machined slots. A specially designed device was used.

Different Fracture Mechanics methodologies were adopted for films' fracture characterization depending on their behavior.

It is well known that if there is no significant crack growth resistance, toughness can be determined from the J-integral value at initiation (J_{Ic}). This value has been extensively used to characterize ductile fracture of polymers [26, 27].

Moreover, other standards also allow using the J integral concept for materials that present cleavage failure (ASTM E1820-13).

Integral J can also be obtained from the maximum load point (J_{max}) by determining the fracture energy up to the maximum of pre-cracked specimens having crack depth/width ratio of $0.45 \leq a/W \leq 0.55$ as follows:

$$J_{\max} = \frac{\eta U_{\max}}{B(W-a)} \tag{2}$$

where U_{max} is the area under the load–deflection curve up to the maximum load point, i.e. the fracture energy up to that point, B the specimen thickness, and η a geometry factor that for DDENT specimens is [28]:

$$\eta = -0.06 + 5.99\left(\frac{a}{W}\right) - 7.42\left(\frac{a}{W}\right)^2 + 3.29\left(\frac{a}{W}\right)^3 \tag{3}$$

J_{max} is not an intrinsic material property. However, it still reflects a critical value for fracture initiation and was adopted here to compare the fracture behavior of the different films. It should also be noted that J values obtained in this work corresponded to plane stress values as the thickness of all films was low. A minimum of five replicates were done for J_{max} determination.

For very ductile fractures, the essential work of fracture (EWF) approach [29–32] can be applied. The aim of this approach is to separate the work performed in the fracture process zone, W_e, from the total work of fracture, W_f, that in ductile polymers is frequently dominated by the plastic work, W_p.

$$W_f = W_e + W_p \tag{4}$$

The work performed in the fracture process zone, the essential work of fracture, is a quasi-material property which only depends on the specimen thickness. The EWF method takes into account that the essential work and the plastic work scale differently:

$$W_f = w_e l B + \beta w_p l^2 B \tag{5}$$

where B is the thickness, l is the uncracked ligament length, β is the shape factor, and w_e and w_p are the specific essential and non-essential work of fracture, respectively. By dividing W_f by the ligament area lB, the specific total work w_f can be expressed as:

$$w_f = w_e + \beta w_p l \tag{6}$$

If the ligament is fully yielded before fracture initiation, the specific essential work can be obtained by testing different ligament lengths and extrapolating the specific total work of fracture to zero ligament length. The EWF method has been widely applied to polymers [33] giving a single fracture parameter that represents the onset of crack propagation.

J_{Ic} and w_e can be compared since they should be identical or very similar, as it has been already confirmed [34–38].

The EWF methodology was used in this work for the film that exhibited completely ductile fracture with full ligament yielding in all samples irrespectively of the ligament length. Twelve samples were used for the application of this methodology.

All mechanical tests were performed in standard laboratory conditions, i.e., at a temperature of 23 ± 2 °C and a relative humidity of $50 \pm 5\%$.

Results and Discussion

Figure 1 shows first and second heating DSC thermograms and their dependence with rolling speed for the films. The glass transition, cold crystallization and melting of the samples are clearly seen in the curves. The films show a sharp glass transition in the form of a hysteresis peak, which is related to a change in the kinetics of unfreezing probably due to a physical aging produced by the thermal treatment above T_g (stretching). Struik has demonstrated that processed plastic products are expected to show these ageing effects [39]. In fact, this hysteresis peak is no longer seen in the second scan. The glass transition temperature T_g increases slightly with rolling speed (see Table 1), probably due to combined ageing effects and chain stretching during processing. This stretching induces orientation of polymer molecules that implies a decrease in free volume between molecules; thus increasing T_g [40, 41].

The exothermic transition around 110 °C is due to the cold crystallization of PLA, which is not significantly affected by the rolling speed. Endothermic peak near 150 °C is the melting peak, which also presents a shoulder. This shoulder peak may derive both from the coexistence of α and α' crystal structures [2, 42] and from the formation of fibrous crystals during stretching [43]. Since the shoulder in the melting peak seems to be more evident as the rolling speed increases, fibrous crystals would be promoted upon stretching in our films. However, the degree of crystallinity is very low for all films (Table 1), indicating that the films' behavior is mostly related to the amorphous phase.

Differences in thermal properties with rolling speed are not seen in the second scan, since processing-induced morphology was erased. Blend's thermal properties are $T_g = 54.9$ °C ± 0.16, $T_c = 111$ °C ± 0.7 and $T_m = 147$ °C ± 0.1. The effect of processing in T_g is corroborated, since T_g of non-stretched blend is lower than T_g of stretched blends.

Figure 2 shows FE-SEM micrographs of cryo-fractured surfaces of the films obtained at different rolling speed (different draw ratio). It is clearly seen that the films presented a two-phase morphology composed of second phase inclusions embedded in the matrix. A significant effect

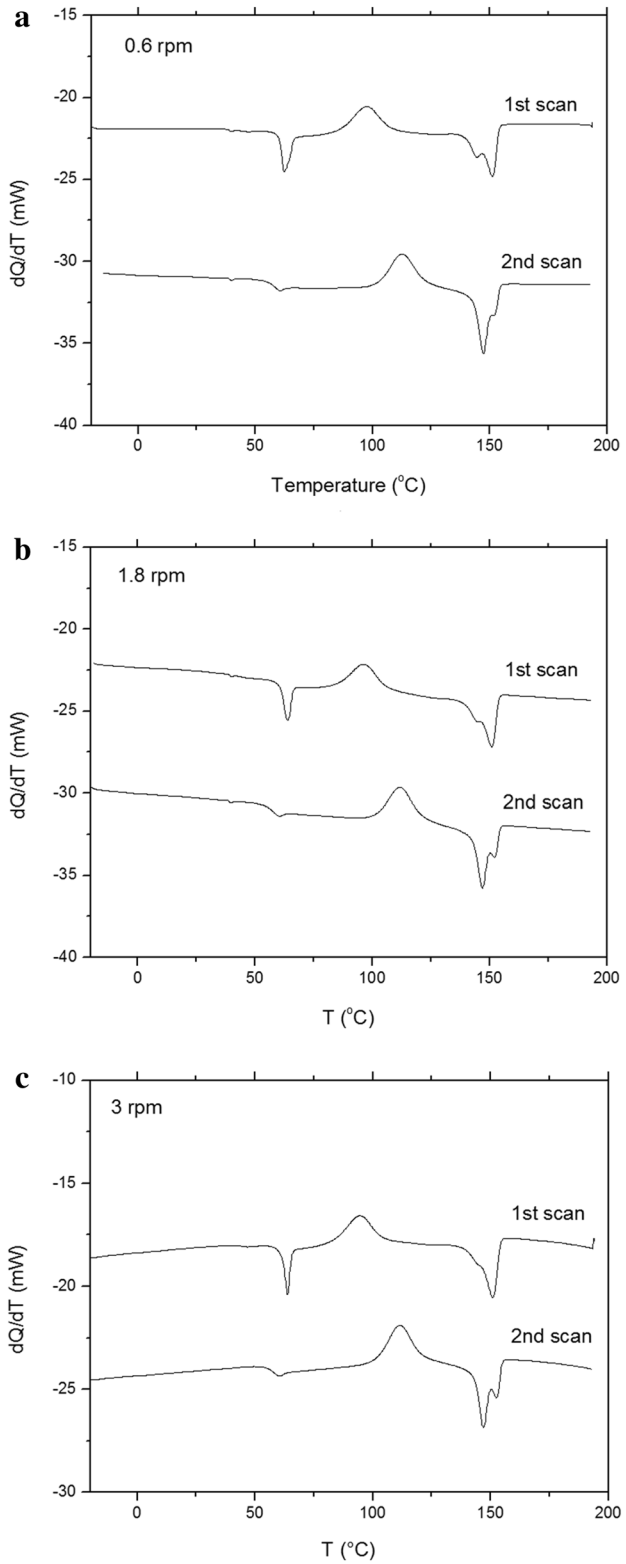

Fig. 1 First and second DSC heating thermograms for the different films obtained at different rolling speed. **a** 0.6 rpm, **b** 1.8 rpm and **c** 3 rpm

Table 1 Thermal properties

Rolling speed	T_g (°C)	T_c (°C)	X_c (%)
0.6	60.3 ± 0.9	110 ± 1.6	1.1 ± 0.6
1.8	62.8 ± 0.4	111 ± 2.9	0.8 ± 0.2
3.0	63.4 ± 0.3	107 ± 2.5	1.1 ± 0.4

of processing conditions (rolling speed) on the morphology of the films was found. While the film obtained at the lowest rolling speed (0.6 rpm) exhibited mostly spherical inclusions, films processed at higher rolling speeds (1.8 and 3 rpm) presented plaques or platelets of the second phase which were found to be thinner as the rolling speed increases.

From SEM micrographs, aspect ratio distributions for second phase inclusions in the different films were also determined with the help of the image processing software *Image J* (NIH). Results are presented in Table 2. A significant increase of the particles' aspect ratio was observed with increasing rolling speed (draw ratio).

The above changes in the films' morphology are expected to have a significant effect on their final performance.

All films displayed ductile behavior in tensile tests exhibiting a yield point, strain softening after this point and a plateau before fracture (Fig. 3). After yielding, a neck which was extended until final fracture was observed on films' samples. Tensile parameters' values as a function of rolling speed are presented in Fig. 4 along with their deviations for the different films investigated.

As it can be observed in Fig. 4a, b, no significant differences in stiffness and yield strength values for the different films were found, being these values intermediate between those for Bio-Flex 6510 and Bio-Flex F 2110.

Strain at break values (Fig. 4c), on the other hand, were significantly lower for the films at higher draw ratio. The high scatter of experimental data was not unexpected, as strain at break is much dependent on the presence of defects in the material and of defects in the surface of the specimens and less reliable than yield strength or modulus.

A remarkable influence of rolling speed (draw ratio) on the films' fracture behavior was observed. Samples of the film obtained at the lowest rolling speed (draw ratio of 2.9) displayed completely ductile behavior in fracture tests, irrespectively of their ligament length. Geometric similarity of load–displacement curves was observed for these samples (Fig. 5a). Therefore, the EWF approach was adopted to characterize fracture behavior in this film.

The film obtained at intermediate rolling speed (draw ratio of 6.3), on the other hand, exhibited different fracture behavior depending on the ligament length (Fig. 5b). Samples with short ligament lengths displayed completely ductile fracture whereas samples with long ligament lengths

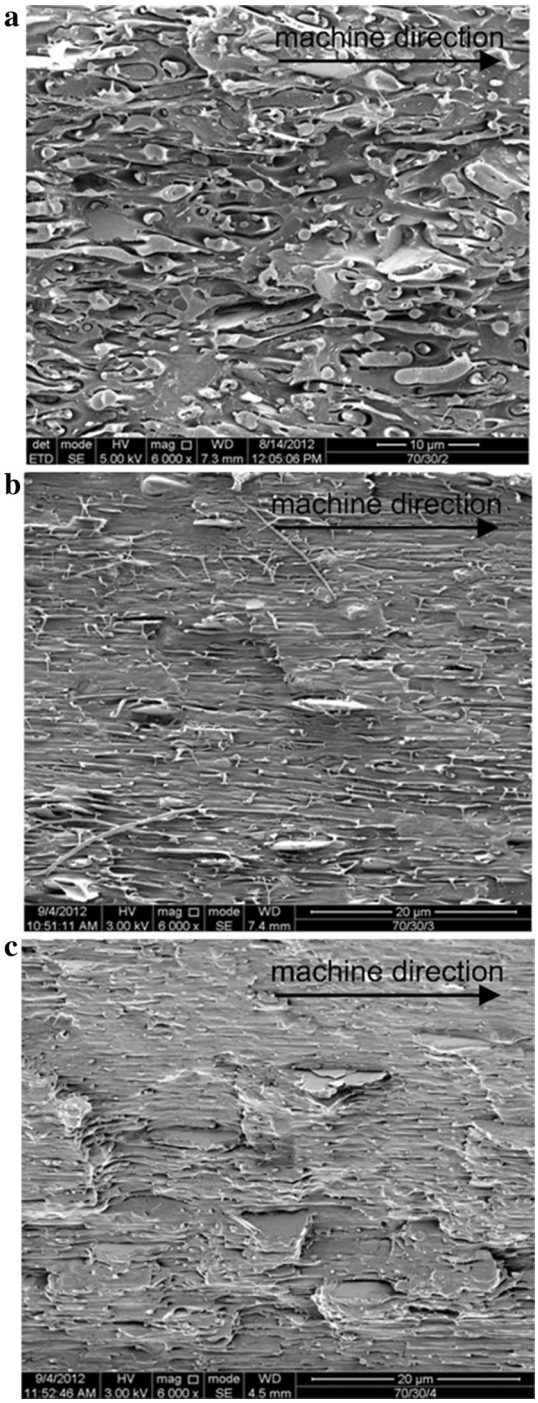

Fig. 2 FE-SEM fractographs of cryofractured samples obtained from cross sections cut in the longitudinal direction (machine direction) of the films processed at different rolling speeds. **a** 0.6 rpm, **b** 1.8 rpm, **c** 3 rpm

exhibited fracture with ductile instability [44], characterized by a precipitous drop of load to zero at a certain point in the load–displacement curve. This change in the fracture behavior with ligament length has been already reported by other authors [45].

Table 2 Aspect ratio values for the second phase inclusions

Rolling speed (rpm)	Aspect ratio (L/l)	
	Average value	Most frequently occurred value
0.6	1.8 ± 0.8	1.4
1.8	5.6 ± 3.6	4.9
3.6	12.1 ± 9.7	6.3

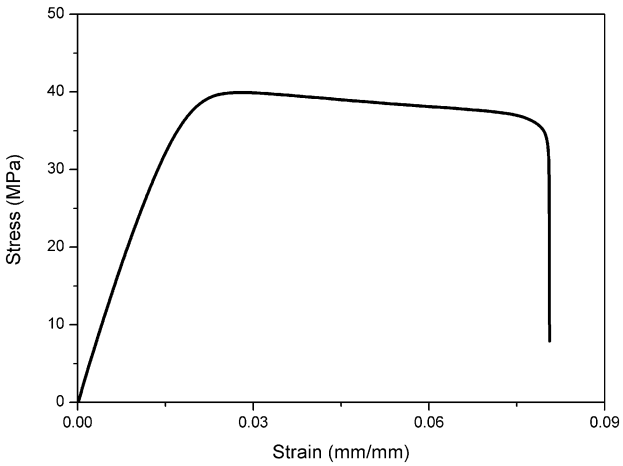

Fig. 3 Typical stress–strain curve for samples of the films obtained at 0.6 rpm

Finally, the film obtained at the highest rolling speed (draw ratio of 11.1) presented the fracture behavior typical of a material in the transition regime: some samples exhibited ductile fracture while others displayed ductile instability (Fig. 5c).

Figure 6 presents the EWF plot for the completely ductile film (the film obtained at 0.6 rpm). A fairly linear correlation between specific work of fracture values and ligament length values was obtained for this film, confirming that the EWF approach could be used to characterize its fracture. The essential and non-essential work of fracture values are also included in Fig. 6.

In order to compare the fracture behavior of all films, the J-integral value at maximum load (J_{max}) was adopted. Values of J_{max} versus rolling speed are presented in Fig. 7 along with their deviations. A significant decrease of the fracture parameter was found for the films obtained at higher rolling speeds (1.8 and 3 rpm).

The influence of rolling speed on fracture performance could be more associated to the significant changes in the films' morphology induced by processing rather than to the blend's composition, as it is always the same in all films. In the load–displacement traces of the film containing nearly spherical second phase inclusions, completely

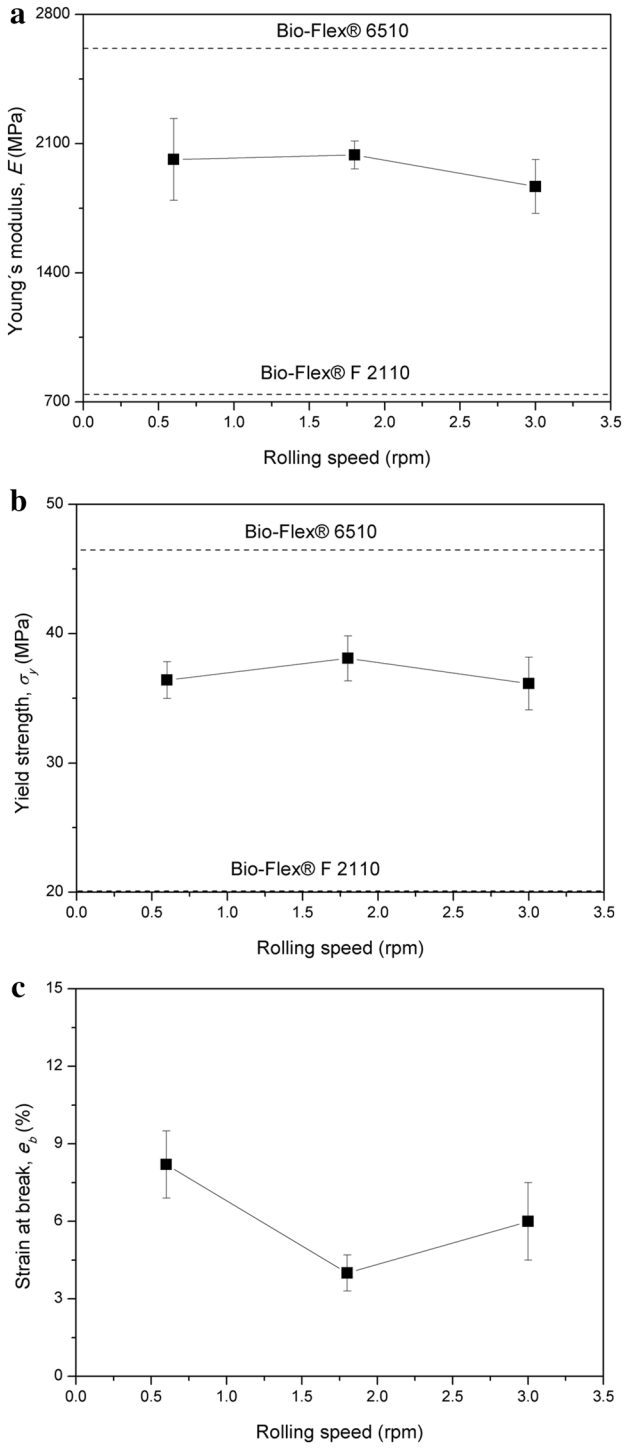

Fig. 4 Tensile properties values as a function of rolling speed for the different films investigated. **a** Young's modulus, **b** yield strength and **c** strain at break

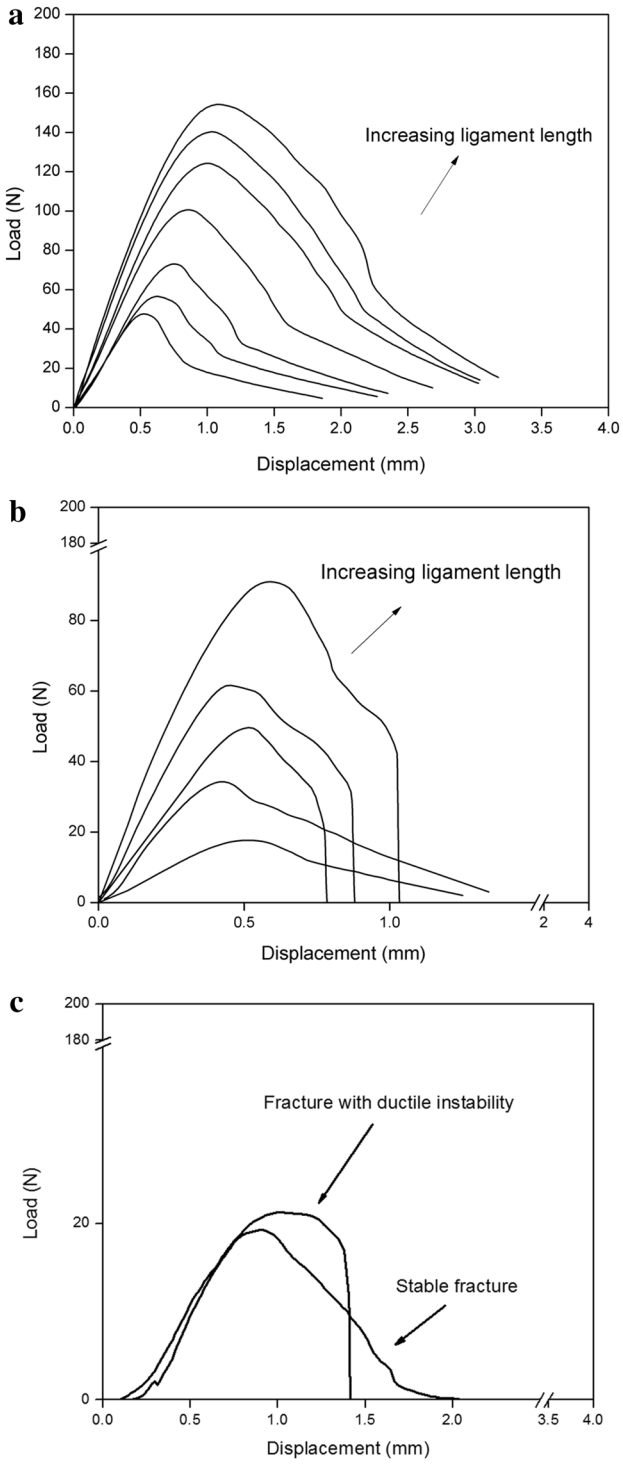

Fig. 5 Load–displacement records for the films obtained at different rolling speeds. **a** 0.6 rpm, **b** 1.8 rpm and **c** 3 rpm

ductile fracture was observed irrespectively of the ligament length. In the films presenting plate-like inclusions, on the other hand, a change in fracture behavior with ligament length or transition regime fracture was found and corresponding lower fracture parameter values were obtained.

For amorphous PLA under quasi-static loading conditions, extensive multiple crazes were observed by Todo and Takayama [46] in the crack-tip region. These crazes dissipate

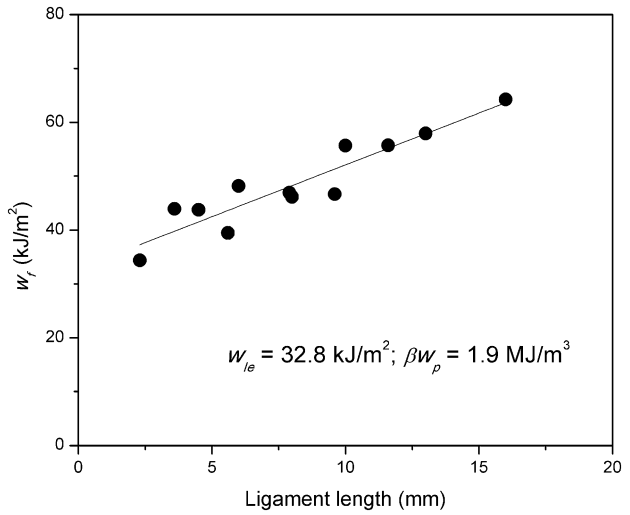

Fig. 6 EWF plot for the film obtained at the lowest rolling speed

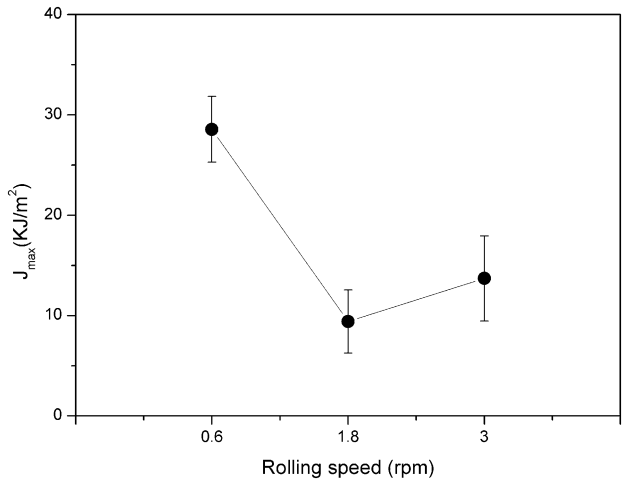

Fig. 7 *J* integral evaluated at the maximum load point (J_{max}) as a function of rolling speed

energy during the fracture process, as it is usually observed in amorphous polymers such as polystyrene.

It has been reported in the literature that large aspect ratio particles oriented normal to the crack propagation direction can induce embrittlement of semi-crystalline polymers by the suppression of multiple crazing [47]. Similarly, sheet-like second phase inclusions (high aspect ratio particles) which existed in the films obtained at higher rolling speeds were oriented in the extrusion direction and hence, normal to the crack propagation direction. In these particles, stresses at the equator would have been much different from those at the pole leading to localized crazing and hence, to films' embrittlement. The nearly spherical particles of the film obtained at the lowest rolling speed, on the other hand, had no orientation leading to uniform stress distribution and hence, crazes could have initiated anywhere and a uniform distribution of crazes (multiple crazing) would have existed.

Conclusions

The tensile and fracture behavior of extruded films based on commercial blends of co-polyester and PLA was investigated, analyzing the effect of the processing through the rolling speed.

It was found that the films were almost amorphous and presented a two-phase morphology composed of softer inclusions embedded in a stiffer matrix, being the morphology of the second phase significantly affected by rolling speed (draw ratio). For the film obtained at the lowest rolling speed, a nearly spherical second phase morphology (low aspect ratio particles) was obtained whereas for the films processed at higher rolling speeds, sheet-like second phase inclusions (high aspect ratio particles) were found.

The processing-induced morphology of the obtained films did not significantly influence the materials' tensile response but it greatly affected the film's fracture behavior. The lowest rolling speed led to a morphology of un-oriented low aspect ratio second phase inclusions that would have stabilized multiple crazing whereas higher rolling speeds led to high aspect ratio inclusions with would have promoted localized crazing and hence, favored films' brittleness.

From the results of this investigation, it is clear that in order to obtain films based on PLA blends at industrial scale (by cast extrusion), the effect of the processing conditions in the films' morphology must be fully controlled as they remarkably influence their final fracture performance.

Acknowledgements The authors want to thank the National Research Council of Argentina (CONICET) and the University of Buenos Aires (UBACyT 20020130200282BA) for financial support of this investigation.

Compliance with Ethical Standards

Conflict of interest The authors confirm that this article content has no conflict of interest.

References

1. Murariu M, Dubois P (2016) Adv Drug Deliv Rev 107:17
2. Saeidlou S, Huneault MA, Li H, Park CB (2012) Prog Polym Sci 37:1657
3. Santana OO, Rodríguez C, Belzunce J, Gámez-Pérez J, Carrasco F, Maspoch ML (2010) Polym Test 29:984
4. Gamez-Perez J (2010) eXPRESS Polym Lett 5:82
5. Arakawa K, Mada T, Park S-D, Todo M (2006) Polym Test 25:628
6. Kawai T, Rahman N, Matsuba G, Nishida K, Kanaya T, Nakano M (2007) Macromolecules 40:9463

7. Takayama T, Todo M, Tsuji H (2011) J Mech Behav Biomed Mater 4:255
8. Hamad K, Kaseem M, Ayyoo M, Joo J, Deri F (2018) Prog Polym Sci 85:83
9. Shirahase T, Komatsu Y, Tominaga Y, Asai S, Sumita M (2006) Polymer 47:4839
10. Oyama HT (2009) Polymer 50:747
11. Hamad K, Kaseem M, Deri F, Ko YG (2016) Mater Lett 164:409
12. Feng F, Ye L (2010) J Macromol Sci B 49:1117
13. Bitinis N, Verdejo R, Cassagnau P, Lopez-Manchado MA (2011) Mater Chem Phys 129:823
14. Rezgui F, Swistek M, Hiver JM, G'Sell C, Sadoun T (2005) Polymer 46:7370
15. Todo M, Arakawa K, Tsuji H, Takenoshita Y (2004) In: Conference 2004, SEM X international congress & exposition on experimental & applied mechanics, Costa Mesa, CA
16. Todo M, Park S-D, Takayama T, Arakawa K (2007) Eng Fract Mech 74:1872
17. Tuba F, Oláh L, Nagy P (2011) Eng Fract Mech 78:3123
18. Imre B (2013) eXPRESS Polym Lett 8:2
19. Paes SS, Yakimets I, Wellner N, Hill SE, Wilson RH, Mitchell JR (2010) Eur Polym J 46:2300
20. Farah S, Anderson DG, Langer R (2016) Adv Drug Deliv Rev 107:367
21. Technical data sheet Bio-Flex F 6510. https://fkur.com/wp-content/uploads/2017/01/TD_BIO-FLEX_F_6510_EN.pdf
22. Technical data sheet Bio-Flex F 2110. https://fkur.com/wp-content/uploads/2016/10/TD_BIO-FLEX_F_2110_en.pdf
23. Sedlarik V, Otgonzul O, Kitano T, Gregorova A, Hrabalova M, Junkar I, Cvelbar U, Mozetic M, Saha P (2012) J Macromol Sci B 51:982
24. Fischer EW, Sterzel HJ, Wegner G (1973) Kolloid-Zeitschrift and Zeitschrift Fur Polymere 251:980
25. Fambri L, Migliaresi C (2010) In: Auras R, Lim L-T, Selke S, Tsuji H (eds) Poly(lactic acid). Synthesis, structures, properties, processing, and applications. Wiley, Hoboken, p 113
26. Plati E, Williams JG (1975) Polym Eng Sci 15:470
27. Bernal C, Rink M, Frontini P (1999) Macromol Symposia 147:235
28. Grellmann W, Reincke K (2004) Mater Test 46:168
29. Cotterell C, Reddel JK (1997) Int J Fract 13:267
30. Mai Y-W, Cotterell B (1986) Int J Fract 32:105
31. Wu J, Mai Y-W (1996) Polym Eng Sci 36:2275
32. Luna P, Bernal C, Cisilino A, Frontini P, Cotterell B, Mai Y-W (2003) Polymer 44:1145
33. Wu J, Mai Y-W, Cotterell B (1993) J Mater Sci 28:3373
34. Clutton E (2001) In: Moore DR, Pavan A, Williams JG (eds) Fracture mechanics testing methods for polymers, adhesives and composites. European Structural Integrity Society, Elsevier, Amsterdam, p 177
35. Mai Y-W, Powell P (1991) J Polym Sci B 29:785
36. Paton CA, Hashemi S (1992) J Mater Sci 27:2279
37. Saleemi AS, Nairn JA (1990) Polym Eng Sci 30:211
38. Levita G, Parisi L, Marchetti A (1994) J Mater Sci 29:4545
39. Struik LGE (1978) Physical aging in amorphous polymers and other materials. Elsevier, Amsterdam
40. Menczel JD, Prime RB, Gallagher PK (2009) In: Menczel JD, Prime RB (eds) Thermal analysis of polymers—fundamentals and applications. Wiley, Hoboken, p 7
41. Lim L-T, Auras R, Rubino M (2008) Prog Polym Sci 33:820
42. Joseph S, Deenadayalan E, Mahanwar PA (2015) J Polym Environ 23:321
43. Yin H-M, Xu H, Zhang J, Chen J-B, Lei J, Xu J-Z, Li Z-M (2015) RSC Adv 5:69016
44. Martinez AB, Gamez-Perez J, Sanchez-Soto M, Velasco JI, Santana OO, Maspoch ML (2009) Eng Fail Anal 16:2604
45. Karger-Kocsis J, Khumalo VM, Bárány T, Mészáros L, Pegoretti A (2013) Compos Interfaces 20:395
46. Todo M, Takayama T (2011) In: Pignatello R (ed) Biomaterials—physics and chemistry. InTech, Rijeka, p 375
47. Cotterell B, Chi JYH, Hbaie K (2007) Eng Fract Mech 74:1054